Received: 26 November 2019 | Revised: 29 April 2020 | Accepted: 25 May 2020

DOI: 10.1002/mrm.28383

FULL PAPER

Magnetic Resonance in Medicine

Free-breathing self-gated 4D lung MRI using wave-CAIPI

Julian A. J. Richter[1,2] | **Tobias Wech**[1] | **Andreas M. Weng**[1] | **Manuel Stich**[1] | **Stefan Weick**[3] | **Kathrin Breuer**[3] | **Thorsten A. Bley**[1] | **Herbert Köstler**[1]

[1]Department of Diagnostic and Interventional Radiology, University Hospital Würzburg, Würzburg, Germany

[2]Comprehensive Heart Failure Center, Würzburg, Germany

[3]Department of Radiation Oncology, University Hospital Würzburg, Würzburg, Germany

Correspondence
Julian A. J. Richter, Department of Diagnostic and Interventional Radiology, University Hospital Würzburg, Oberdürrbacher Str. 6, 97080 Würzburg, Germany.
Email: richter_j1@ukw.de

Funding information
Bundesministerium für Bildung und Forschung, Grant/Award Number: 01EO1504, Siemens Healthcare GmbH

Purpose: The aim of this study was to compare the wave-CAIPI (controlled aliasing in parallel imaging) trajectory to the Cartesian sampling for accelerated free-breathing 4D lung MRI.

Methods: The wave-CAIPI k-space trajectory was implemented in a respiratory self-gated 3D spoiled gradient echo pulse sequence. Trajectory correction applying the gradient system transfer function was used, and images were reconstructed using an iterative conjugate gradient SENSE (CG SENSE) algorithm. Five healthy volunteers and one patient with squamous cell carcinoma in the lung were examined on a clinical 3T scanner, using both sampling schemes. For quantitative comparison of wave-CAIPI and standard Cartesian imaging, the normalized mutual information and the RMS error between retrospectively accelerated acquisitions and their respective references were calculated. The SNR ratios were investigated in a phantom study.

Results: The obtained normalized mutual information values indicate a lower information loss due to acceleration for the wave-CAIPI approach. Average normalized mutual information values of the wave-CAIPI acquisitions were 10% higher, compared with Cartesian sampling. Furthermore, the RMS error of the wave-CAIPI technique was lower by 19% and the SNR was higher by 14%. Especially for short acquisition times (down to 1 minute), the undersampled Cartesian images showed an increased artifact level, compared with wave-CAIPI.

Conclusion: The application of the wave-CAIPI technique to 4D lung MRI reduces undersampling artifacts, in comparison to a Cartesian acquisition of the same scan time. The benefit of wave-CAIPI sampling can therefore be traded for shorter examinations, or enhancing image quality of undersampled 4D lung acquisitions, keeping the scan time constant.

KEYWORDS
free-breathing, lung, self-gated, wave-CAIPI

1 | INTRODUCTION

The lung is an especially challenging organ to image with MR, as the acquisition is typically impaired by respiratory and cardiac motion. In addition, the fast T_2^* decay of the MR signal and the inherently low proton density of lung tissue complicates lung MRI. The easiest way to avoid artifacts arising from respiration is a breath-hold examination. However, patients often have a limited breath-hold capability, posing a severe restriction to the available acquisition time. Another approach is respiratory gating by means of image-based methods,[1,2] or using additional external hardware.[3] In addition, the center of k-space can be exploited as a navigator signal.[4-6] Although some non-Cartesian k-space trajectories inherently measure this (direct current) DC signal in each repetition,[7] a small increase in measurement time has to be invested in Cartesian and in wave-CAIPI (controlled aliasing in parallel imaging). The big advantage of these self-gating techniques is that they do not require any additional hardware, which saves time during patient preparation and increases patient comfort. Furthermore, retrospective gating allows for individual adjustment of gating parameters after the acquisition. Finally, the implementation of retrospective self-gating requires only minor modifications to existing pulse sequences. However, even with respiratory self-gating, acquisition times should be kept as short as possible, as long scan times bear an increased risk of involuntary patient movement, ultimately leading to degraded image quality. Furthermore, as available time slots in clinical routine are very limited, acceleration of the acquisition enables a higher patient throughput.

The Cartesian k-space trajectory is used most prominently in clinical routine. However, other k-space trajectories may be better suited for accelerated imaging, which is of utmost importance to improve patient comfort. Recently, wave-CAIPI has been proven to be a very effective method for volumetric acquisitions, accelerated by parallel imaging.[8-12] In this work, the wave-CAIPI k-space trajectory is used in a self-gated FLASH pulse sequence for dynamic lung imaging, to make better use of receive coil sensitivity variations in all three spatial dimensions.

A key difference to previous reports that used the wave-CAIPI technique is—apart from the target application—the phase-encoding scheme. The wave-CAIPI k-space trajectory is typically combined with a regular, 2D CAIPI-shifted undersampling pattern. In a work by Chen et al,[13] a variable density sampling and radial view ordering[14] scheme was used. To avoid large gaps in k-space after retrospective gating, the phase-encoding scheme in this work was randomized using a nonuniform density distribution that oversamples the center of k-space.

This work combines a randomized self-gated FLASH pulse sequence with the wave-CAIPI k-space trajectory to acquire high-quality, dynamic 3D images of the human lung during free breathing. The proposed method is especially interesting for radiotherapy treatment planning,[15,16] as respiration-induced tumor motion needs to be carefully evaluated before treatment. For different acquisition times, the wave-CAIPI sequence is compared to a Cartesian sequence with, apart from the k-space trajectory, identical parameters.

2 | METHODS

2.1 | Setup

The wave-CAIPI k-space trajectory was implemented in a 3D FLASH pulse sequence by playing out sinusoidal gradient oscillations on both phase-encoding axes during readout. The oscillations were shifted with respect to one another by a phase of $\pi/2$, leading to helically shaped readout lines in k-space. In this work, a fixed number of gradient oscillations $N_{\text{wave}} = 4$ and a maximum gradient wave amplitude $A_{\text{wave}} = 6\ \text{mT/m}$ was chosen. To acquire the k-space center signal ("DC signal"), which was used as a respiratory navigator signal, the ADC was opened for a short time immediately after the nonselective RF excitation pulse. A schematic pulse sequence diagram is shown in Figure 1A. For all examinations, both wave-CAIPI and Cartesian reference scans were performed, using identical sequence parameters, apart from the additional gradient oscillations for the wave-CAIPI technique. Images were acquired with an isotropic resolution of 2.23 mm and a k-space matrix of size 224 × 224 × 112-144. Further relevant sequence parameters were FOV = 500 × 500 × 250-321 mm^3, TR = 4.8 ms, TE = 1.9 ms, flip angle = 5°, readout bandwidth = 350 Hz/pixel, corresponding to a readout duration of 2.86 ms. Readout was always chosen to be in the head–foot direction. All examinations were performed with an 18-channel body coil array, in combination with a spine coil array with 12-16 channels activated.

The order of the phase-encoding steps was randomized with respect to nonuniformly distributed, 2D pseudo-random numbers, to avoid synchronization between phase encoding and breathing motion.[15,17] Hence, 2D pseudo-random numbers within the 2D range of ([0, 1], [0, 1]) were generated by a Mersenne-Twister algorithm,[18] as implemented in the C++ standard library, using a normal distribution with a width of $\sigma = 0.3$. The resulting distribution was rescaled by the number of phase-encoding steps in both dimensions. The density distribution that was used is displayed in Figure 1C. A typical full sampling pattern of an 8-minute acquisition before respiratory gating is shown in Figure 1D.

To quantitatively evaluate and compare image quality, 4D lung MR scans were performed on 5 healthy volunteers, using both sampling strategies. In addition, 1 patient (male, 65 years old) with known squamous cell carcinoma in the lung was examined, and respiration-induced tumor movement was assessed. For both samplings, wave-CAIPI and Cartesian, the total acquisition time was set to T_{Acq} = 08:01-10:18 minutes,

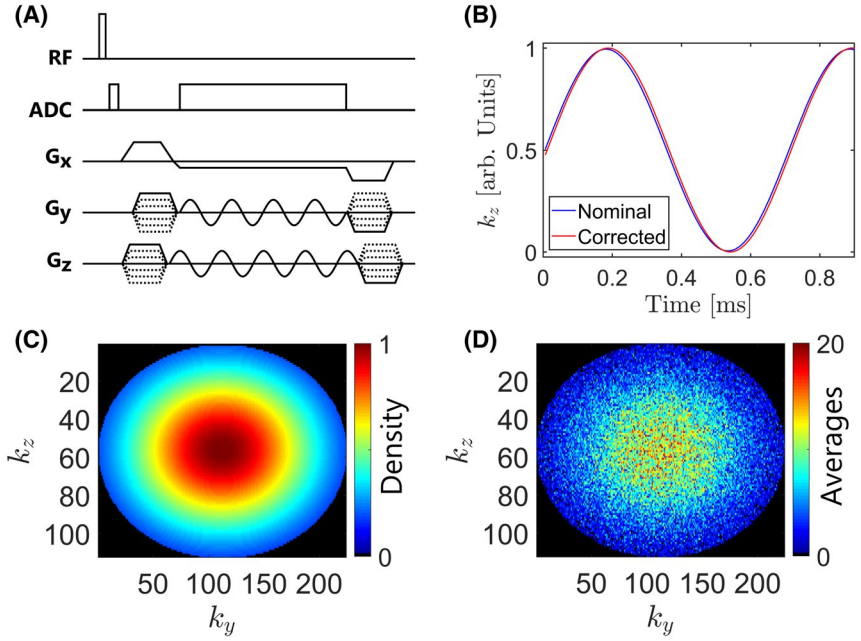

FIGURE 1 A, Diagram of the self-gated gradient echo pulse sequence with wave-CAIPI (controlled aliasing in parallel imaging) sampling. For respiratory self-gating, the ADC acquires the center of k-space immediately after the nonselective RF excitation. The phase-shifted sinusoidal gradient oscillations on the phase-encoding axes generate the helical wave-CAIPI k-space trajectory. B, Correction of k-space trajectory errors, caused by gradient system imperfections. C, Density distribution used for randomization of the phase-encoding order. D, Full sampling pattern of an 8-minute acquisition, before retrospective gating

leading to a moderate average undersampling rate of $R \approx 1.5$ in the images after respiratory self-gating, which was considered to provide adequate reference images for the later comparison with accelerated scans. For the calculation of sensitivity maps, a low-resolution, Cartesian reference scan with increased FOV in the coronal plane was performed.

All measurements were performed on a 3T clinical scanner (MAGNETOM Prisma^{fit}; Siemens Healthcare, Erlangen, Germany). The in vivo study was approved by our institution's ethics committee, and informed, written consent was obtained from each subject before measurement.

2.2 | Reconstruction

Regardless of the used k-space trajectory, the first step for image reconstruction is sorting the data, acquired in pseudo-random order, into different breathing states. To this end, the DC signal measured by the ADC directly after the excitation pulse is used as a navigator signal.[4-6] In the absence of spatial encoding, this signal is proportional to the total amount of protons within the imaged object, weighted by the sensitivity profiles of the respective receive coils. The signal of a single receive coil near the lung/liver interface was manually selected and band-pass-filtered to smooth the signal and to remove signal variations corresponding to the periodic cardiac motion. The remaining signal variations of that coil then arise from tissue (liver) moving in and out of the range of sensitivity of the coil, and therefore serve as a respiratory navigator. An exemplary self-gating signal is displayed in Figure 2 for a volunteer examination. The measured data were binned into partially overlapping breathing states, with the requirement that all breathing states contain about 21% of all acquired

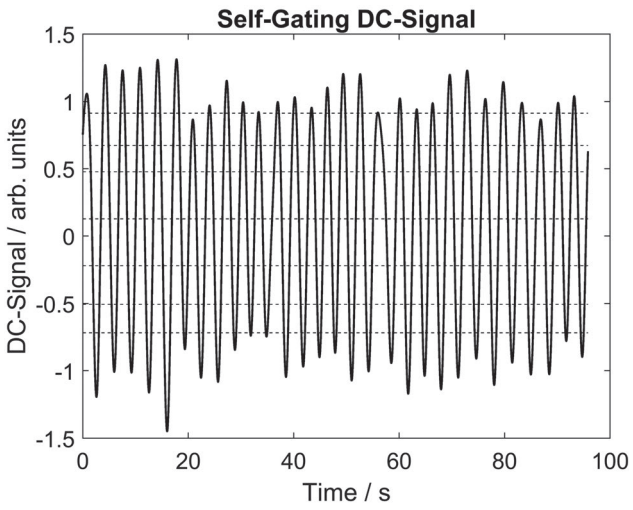

FIGURE 2 Self-gating (direct current) DC signal of a volunteer measurement. The center of k-space, measured by a receive coil near the lung/liver interface, serves as a respiratory navigator signal. The acquired data are distributed into eight breathing states (dashed horizontal lines). Boundaries were chosen to be "soft" (ie, adjacent breathing states overlap by a certain amount [not shown])

data. The respiratory cycle was resolved in eight breathing states, which is a typical range for dynamic 3D lung acquisitions.[7,15] This approach ensures that all k-space bins (corresponding to the breathing states) contain a sufficient amount of data for a stable parallel imaging reconstruction. Before respiratory gating, the first 2500 readouts were discarded, to be sure to achieve a steady-state magnetization.

Gradient system imperfections cause gradient discrepancies, such that the actually played-out sinusoidal gradient oscillations of the wave-CAIPI are a distorted version of the nominal gradients (ie, as designed in the pulse program).[19-22]

Depending on the gradient axis, the real sinusoidal gradient oscillations differ from the theoretical waveforms by a time delay in the order of 6 μs and magnitude alterations of about 1%. The discrepancy between the theoretical input gradient and the gradient that is actually played out leads to inaccuracies in the k-space trajectory (as displayed in Figure 1B), consequentially deteriorating the image quality of the wave-CAIPI acquisitions. The gradient system transfer function characterizes this gradient system behavior and can therefore serve as a correction of the latter problem during reconstruction.[19-22] The gradient system transfer function of the MR scanner was determined in additional phantom measurements. To this end, the phase evolution of the MR signal was measured in two parallel slices, while triangular input gradients were played out on the gradient axis perpendicular to the excited, parallel slices. Separate measurements for the three individual gradient axes were performed. A good estimate of the true k-space trajectory can be obtained by using only the self-terms of the gradient system transfer function.

After retrospective data sorting into breathing states and k-space trajectory correction, the images were reconstructed using an iterative CG SENSE approach.[23,24] Sensitivity maps were calculated using the Berkeley Advanced Reconstruction Toolbox.[25] Reconstruction times were between 45 and 90 minutes for eight breathing phases, depending on the degree of undersampling. Especially for comparisons of two different imaging techniques, a fair choice for the regularization parameter, in this case, the stopping criterion for the iterative SENSE reconstruction, needs to be defined. In this work, a criterion based on the actual image noise was formulated. From an additional scan, noise correlations in the different receiver coil elements were calculated for all volunteer examinations. For the noise measurement, the same pulse sequence setup as for actual imaging was used, with the RF amplitude set to zero. Therefore, only noise was measured in each receive channel. This measurement of noise correlations can be performed in only a few seconds. Subsequently, properly correlated, artificial noise can be generated using the method proposed by Robson et al.[26] From the noise-only data, a noise covariance matrix describing noise correlations between the individual channels was calculated. The noise covariance matrix was used to generate artificial but authentic noise samples, to simulate a fully sampled, multichannel, noise-only scan with the same k-space matrix as for actual imaging. To obtain the image noise estimate from the noise-only k-space, a Fourier transformation was performed, and coil combination was done, taking into account the coil sensitivity maps. The noise estimate r_{Noise} is then calculated as the L_2-norm of the coil-combined noise image, as follows:

$$r_{\mathrm{Noise}} = \sqrt{\sum_{i=1}^{N_{\mathrm{px}}} \left| \sum_{k=1}^{N_{\mathrm{ch}}} m_{ik} C_{ki}^{*} \right|^2},$$

where C^* is the complex conjugate transpose of the coil sensitivity matrix; m denotes the individual coil images; N_{ch} is the number of channels; and N_{px} is the number of image pixels. Iterations of the CG SENSE algorithm were performed until the CG residual r_{CG} obeyed $r_{\mathrm{CG}} < c \cdot r_{\mathrm{Noise}}$, where the factor c dictates the compromise between residual aliasing artifacts and image noise. For the in vivo studies, the parameter was set to be in the range of 0.3-0.5, whereas for the phantom-based SNR calculations, $c = 0.3$ was chosen. The same value of c was chosen for the respective Cartesian and wave-CAIPI reconstructions. Based on the proposed criterion, the algorithm was stopped in the transition phase of the typical L-shaped function of the logarithm of the CG residual, plotted against the iteration number, as suggested in the work by Qu et al.[27]

2.3 | Image analysis

The wave-CAIPI and Cartesian acquisitions were retrospectively accelerated. For this purpose, shorter scans were simulated by discarding data acquired at the end of the measurement, such that only a certain period of time (starting after establishing a steady-state magnetization) was kept. To assess the image quality for different accelerations, the normalized mutual information (NMI) and the RMS error (RMSE) were calculated for each breathing state as a function of acquisition time and used to quantify image similarity between retrospectively accelerated acquisitions and their respective references.[15,28,29] The reference images were chosen to be the images of the individual breathing states, before retrospective acceleration. For this approach to work, the initially determined gating windows were kept fixed for all accelerations. The normalized mutual information of two discrete variables X and Y was calculated as

$$\mathrm{NMI}(X,Y) = \frac{I(X,Y)}{\sqrt{H(X) \cdot H(Y)}},$$

where $I(X,Y)$ is the mutual information between X and Y, and $H(X)$ and $H(Y)$ denote the entropy of X and Y, respectively. The NMI describes the amount of information that can be obtained about variable X by measuring the variable Y. It is therefore suited as a similarity measure to compare different accelerated images with their respective reference. In addition to the NMI, the RMSE between the reference image and the accelerated images was calculated.

The SNR ratio $r_{\mathrm{SNR}} = \mathrm{SNR}_{\mathrm{wave-CAIPI}}/\mathrm{SNR}_{\mathrm{Cartesian}}$ and g-factors were calculated on a pixel-by-pixel basis for accelerated wave-CAIPI and Cartesian phantom experiments by means of the pseudo multiple replica method.[26] To this end, 100 reconstructions were performed, each time adding artificial, properly correlated, and scaled noise to the acquired data. The phantom images were acquired using the same

density-weighted sampling scheme as for the dynamic lung images. The sampling pattern was adapted to mimic a typical k-space sampling pattern for a 1-minute 4D-lung MRI after respiratory gating (fraction of missing k-space lines ~92%). The phantom consisted of two stacked canisters, containing NaCl and $NaH_2PO_4*2H_2O$ in water, respectively. As the phantom is not representative for actual lung tissue, absolute SNR values do not necessarily correspond to SNR in in vivo measurements. However, the SNR ratio, comparing wave-CAIPI and Cartesian sampling, is not affected by relaxation parameters and provides an adequate measure of SNR gain. The SNR calculation was performed using phantom measurements, as the final undersampling patterns of in vivo scans are different using retrospective self-gating. The same undersampling pattern was used for the wave-CAIPI and the Cartesian reconstruction. This avoids any possible effects due to different sampling patterns and is not possible for retrospectively gated in vivo data. The phantom-based approach also prevents errors in $r_{SNR} = SNR_{wave-CAIPI}/SNR_{Cartesian}$ due to motion, and enables a comparison on a pixel-by-pixel basis.

Furthermore, g-factor maps were calculated for accelerated wave-CAIPI and Cartesian 4D lung scans, also using the pseudo multiple replica method. To assess differences between wave-CAIPI and Cartesian sampling in the g-factor maps, the same undersampling pattern was simulated for the in vivo images as follows: The respective full data sets (without retrospective acceleration; scan time ~8 minutes) were reconstructed using the CG SENSE algorithm. The resulting artifact-free images were resampled retrospectively, to simulate a fully sampled in vivo scan. These artificially fully sampled data sets were then undersampled, using the same random undersampling pattern for both sampling techniques.

3 | RESULTS

Using the self-terms of the gradient system transfer function, image artifacts arising from gradient imperfections were effectively suppressed, as demonstrated in Figure 3 for a sagittal slice of a volunteer measurement.

A comparison of retrospectively accelerated images for Cartesian and wave-CAIPI sampling is shown in Figure 4. For an acquisition time of 8:01 minutes, both techniques result in good image quality. Especially in the case of high acceleration (down to 1 minute), the Cartesian images exhibit visible residual undersampling artifacts, whereas the artifact level is reduced using the wave-CAIPI technique. A more detailed comparison of accelerated images in three different orientations is displayed in Figure 5 for an acquisition time of 2 minutes.

Figure 6A-E presents box plots of calculated NMI values for all 5 healthy volunteer examinations; the average of

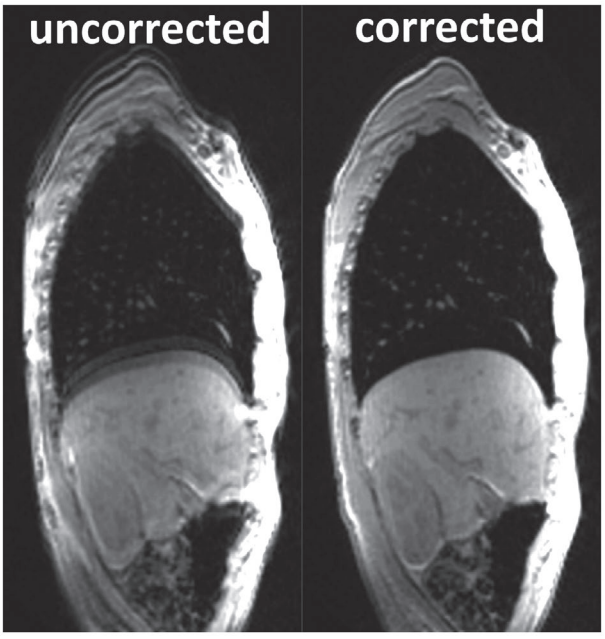

FIGURE 3 Comparison of a sagittal slice of a wave-CAIPI acquisition before and after gradient imperfections were accounted for. Gradient inaccuracies lead to considerable artifacts in the frequency-encoding direction (head–foot). The correction method using the gradient system transfer function successfully suppresses image artifacts arising from gradient imperfections

NMI values was determined over the eight different breathing states. Median NMI values of the wave-CAIPI acquisition are consistently higher than the Cartesian NMI medians. Scatterplots of the NMI and the RMSEs of all volunteer measurements are shown in Figure 7. Most (91%) of the calculated RMSE values of the accelerated wave-CAIPI images are lower than the RMSEs for the Cartesian images; most of the individual RMSE values lie below the identity line in Figure 7A. As shown in Figure 7B, 97% of the individual NMI values lie above the identity line (ie, wave-CAIPI scans exhibit higher NMI values). Especially for small acquisition times, which correspond to higher RMSE and lower NMI levels, the difference between the two sampling schemes is more pronounced. For the images with an acquisition time of 2 minutes, the mean RMSE value for wave-CAIPI is 6.51 ± 1.78 and for Cartesian sampling, and the mean RMSE is 7.82 ± 1.79, in arbitrary signal intensity units. On average, RMSE values were $18.9\% \pm 13.2\%$ lower, and NMI values were $10.2\% \pm 7.3\%$ higher for the wave-CAIPI, compared with Cartesian sampling.

Figure 8A,B show 4D MR and PET/CT images of a patient with squamous cell carcinoma in the lung. The 3-minute wave-CAIPI 4D MRIs show superior image quality, compared with the 3-minute Cartesian acquisitions. No relevant respiratory motion-induced displacement of the tumor can be observed, as displayed in Figure 8C for the 3-minute wave-CAIPI MRI. As a result, in the process of radiotherapy

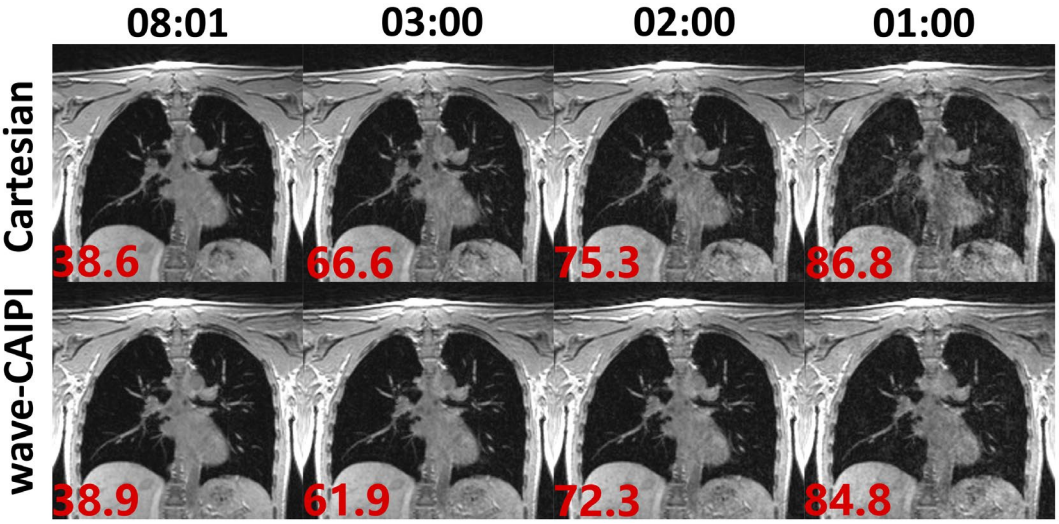

FIGURE 4 Comparison of a coronal slice of a Cartesian and a wave-CAIPI image for different acquisition times at end-expiration. For smaller acquisition times, artifacts in the Cartesian images are more prominent than in the wave-CAIPI images. The percentage of missing k-space lines of the individual images are stated in the respective lower-left corners

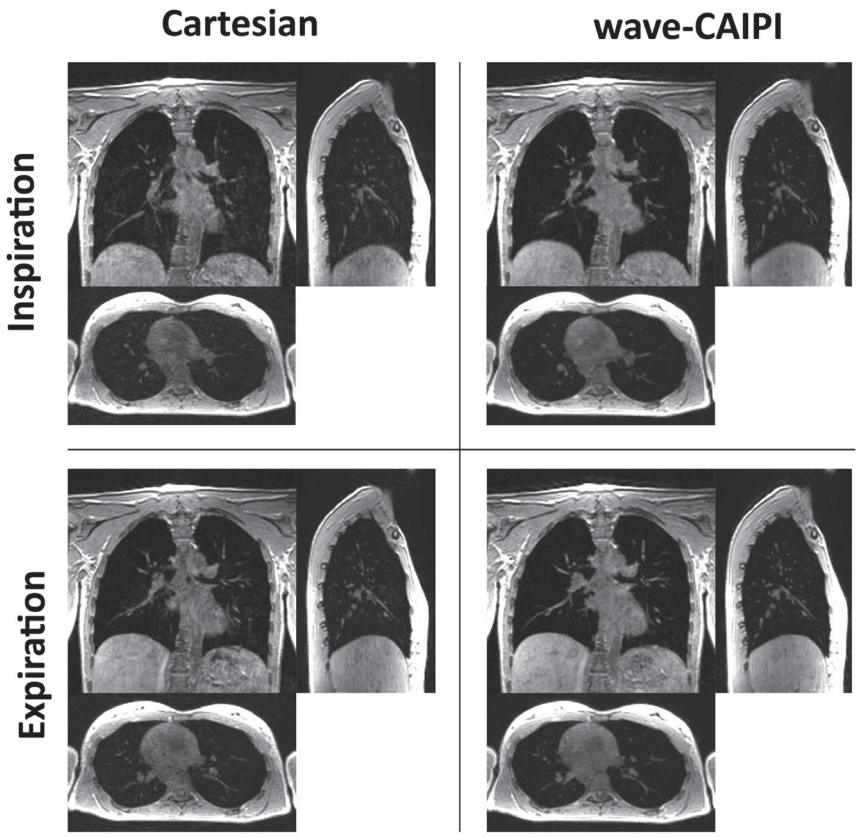

FIGURE 5 Comparison of three different orientations of a Cartesian and a wave-CAIPI image at inspiration and expiration with an acquisition time of 2 minutes. Residual undersampling artifacts are less pronounced in the wave-CAIPI images

treatment planning, the safety margins around the tumor do not need to be increased due to respiration.

The SNR ratio $r_{\mathrm{SNR}} = \mathrm{SNR}_{\mathrm{wave-CAIPI}}/\mathrm{SNR}_{\mathrm{Cartesian}}$ that was calculated in the phantom for the two trajectories is presented in Figure 9A, binned according to the Cartesian g-factor in the corresponding pixels. An exemplary slice of the median-filtered SNR ratio map is displayed in Figure 9B. The average SNR gain of wave-CAIPI was $r_{\mathrm{SNR}} = 1.14 \pm 0.31$. Calculations of the g-factor (using the same set of replicas as for the SNR measurement) yielded an average g-factor of $g_{\mathrm{mean}} = 1.21$ for wave-CAIPI in the phantom. In the Cartesian case, the average g-factor was $g_{\mathrm{mean}} = 1.34$ in the phantom. g-Factor maps for a simulated 2-minute in vivo scan are presented in Figure 9C.

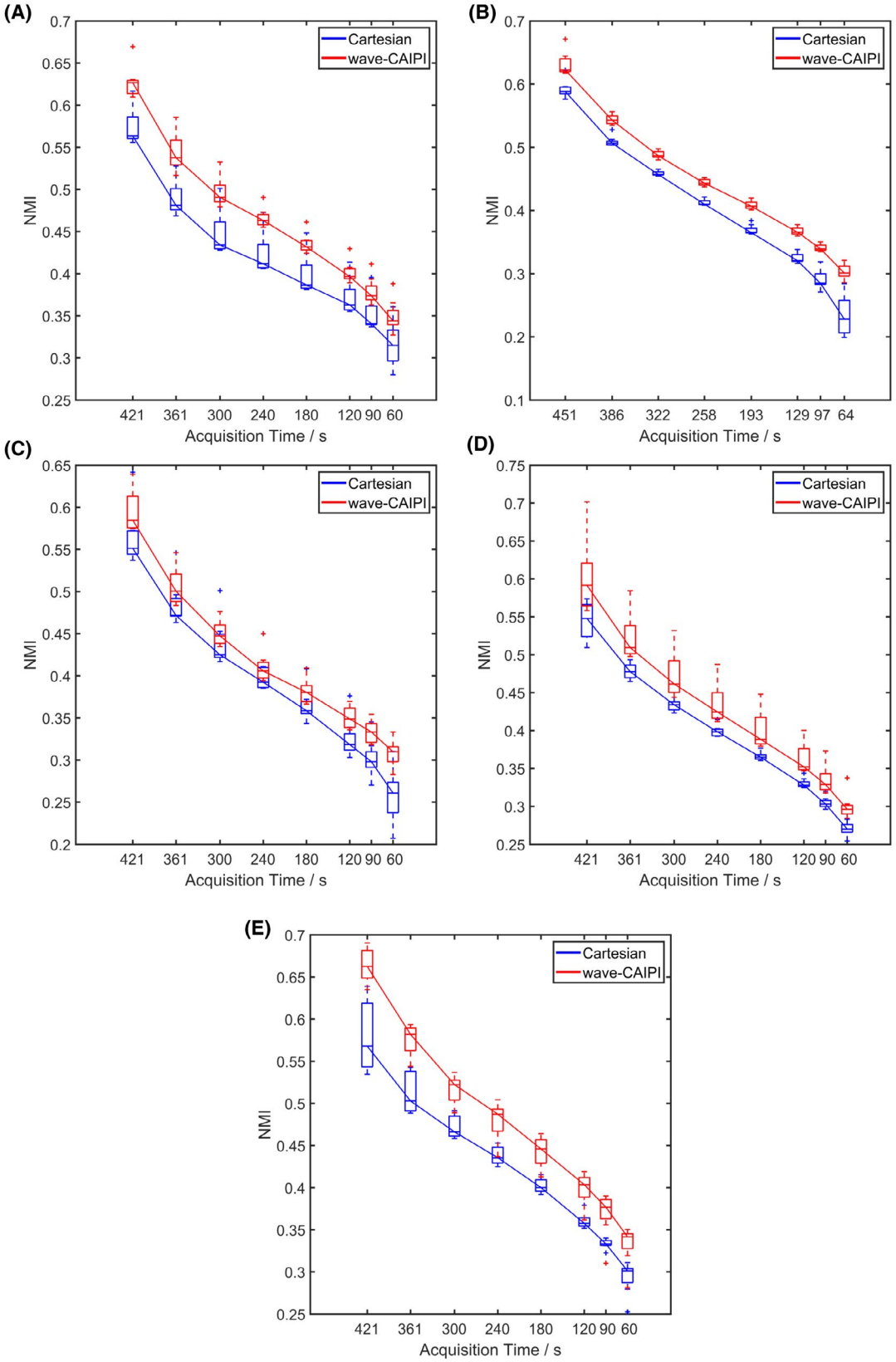

FIGURE 6 A-E, Box plots of the normalized mutual information (NMI) between accelerated images and their respective references for 5 volunteer examinations. The average is performed over the individual breathing states. Median NMI values of the wave-CAIPI are consistently above the Cartesian NMI values

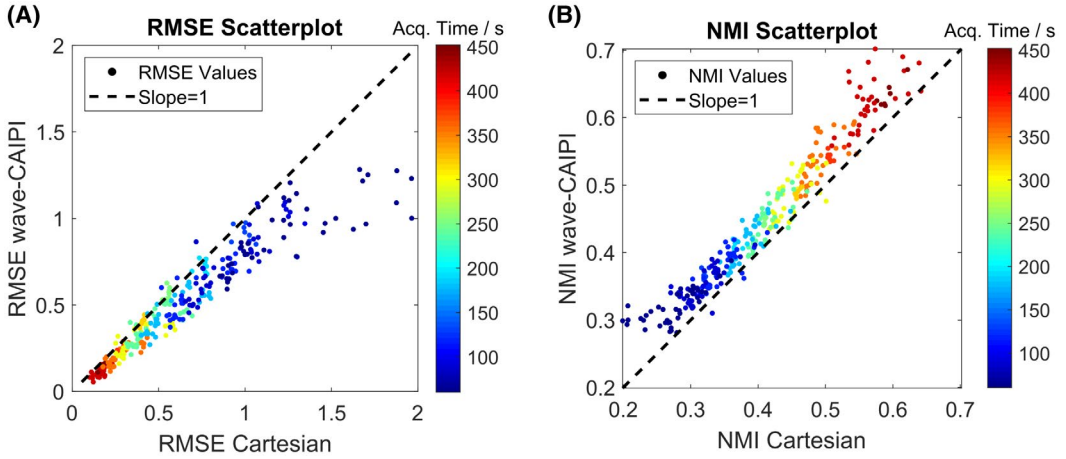

FIGURE 7 Scatterplots of the RMS error (RMSE) (A) and the NMI (B) to compare wave-CAIPI and Cartesian acquisitions. In both (A) and (B), the dashed lines represent the respective identity lines, with slope = 1

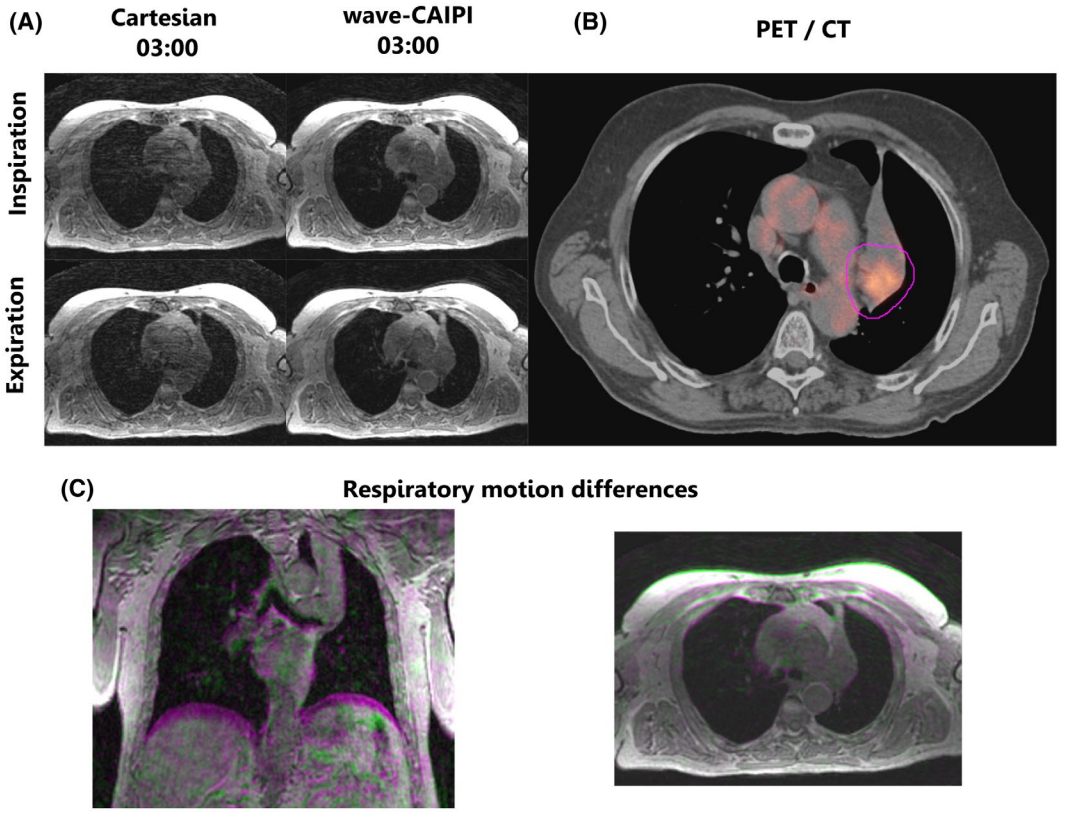

FIGURE 8 A, Axial slice of a patient with squamous cell carcinoma in the lung in inspiration and expiration, acquired with Cartesian and wave-CAIPI sampling. B, The PET/CT acquisition of a similar slice as in (A), with target region for radiotherapy (magenta line). C, Respiratory motion differences in coronal and axial orientation, determined from a 3-minute wave-CAIPI scan. Differences between inspiration and expiration are color-encoded (magenta/green)

4 | DISCUSSION

The results of the patient examination indicate that, using the wave-CAIPI sampling, the image quality of accelerated acquisitions can be enhanced while keeping the scan time constant. In the presented case, no relevant displacement of the tumor could be observed during respiration. An important application of the proposed method would be in the context of radiotherapy treatment planning. It is very important in radiotherapy not only to ensure tumor coverage with the prescribed dose but also to spare organs at risk (eg, lung, liver, heart). For this purpose, safety margins around the tumors are used in the target volume definition process to guarantee coverage. If tumor motion is not considered at all, very large margins have to be used, resulting

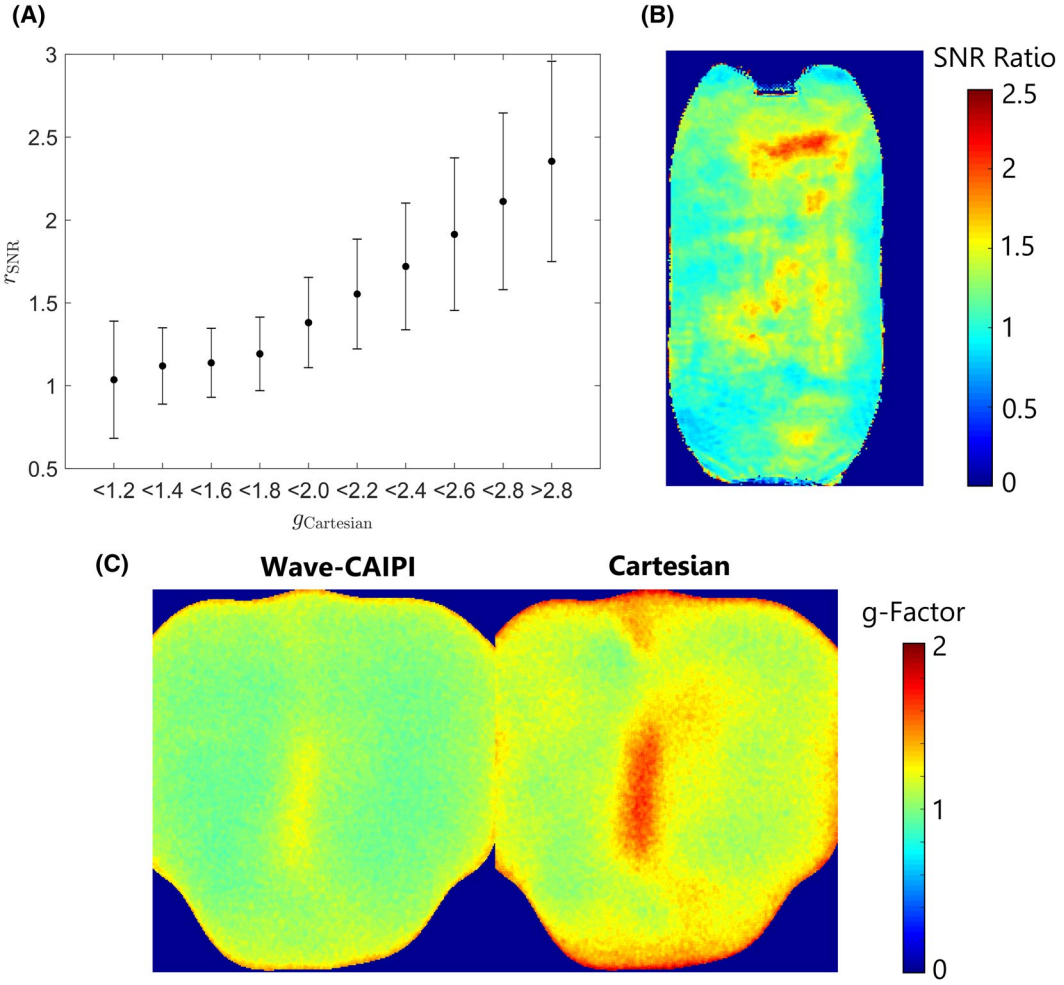

FIGURE 9 A, The SNR ratio $r_{SNR} = SNR_{wave-CAIPI}/SNR_{Cartesian}$ in pixels of a phantom, binned according to the corresponding g-factors of the Cartesian image. In pixels with higher g-factor, the SNR gain by using wave-CAIPI is larger. The phantom consisted of two stacked canisters, containing NaCl and NaH_2PO_4*$2H_2O$ in water, respectively. B, Slice of the SNR ratio map ($SNR_{wave-CAIPI}/SNR_{Cartesian}$) in coronal orientation. C, g-Factor map of a 2-minute in vivo scan, comparing wave-CAIPI and Cartesian sampling

in a high probability of radiation-induced pneumonitis, for example.[30] Different treatment planning concepts are used to create target volumes that are influenced differently by more extreme respiration states.[30,31] Tumor delineation depends substantially on image quality. Consequently, accelerated images acquired with the wave-CAIPI sampling technique are superior over Cartesian ones. In the present case, safety margins around the tumor do not need to be increased due to respiratory motion. Moreover, the superior soft-tissue contrast compared with CT can lead to further dose reductions, especially for the identification of moving lesions in the pancreas, for example.[32]

The calculated normalized mutual information as a function of acquisition time is used as a quantitative measure to capture the similarity of the accelerated images to their respective references (initial full-duration scan; no retrospective scan-time reduction). For each breathing state, a series of images with decreasing acquisition time is generated and the NMI is calculated. The respiratory gating windows are fixed for all accelerated images, to ensure comparability of images with different acquisition times. Median NMI values of the wave-CAIPI scans lie consistently above those of the Cartesian scans, indicating a lower loss of image information due to acceleration. The scatterplots of RMSE and NMI in Figure 7 show that the accelerated wave-CAIPI images exhibit smaller discrepancies to the reference images compared with the Cartesian case. This is supported by phantom-based SNR ratio calculations. The SNR advantage of $r_{SNR} = 1.14 \pm 0.31$ for the wave-CAIPI approach leads to a more well-posed CG SENSE reconstruction, which reduces residual noise enhancement in the final images. In Figure 9A, the SNR ratio in the individual pixels of the phantom images are binned according to the Cartesian g-factor in the respective pixel. The SNR gain by using the wave-CAIPI is larger in regions where the Cartesian image exhibits a large g-factor. In the phantom, g-factor calculations of the used setup yielded average g-factors of $g_{wave} = 1.21$ for the wave-CAIPI, compared with $g_{Cartesian} = 1.34$ for the Cartesian imaging. The g-factor maps of the simulated 2-minute 4D-lung

scans in Figure 9C also show reduced noise enhancement in the wave-CAIPI case. In Bilgic et al,[8] the wave-CAIPI technique was shown to yield an average g-factor of $g_{wave} = 1.03$, compared with $g_{Cartesian} = 1.42$ in the 2D-CAIPI Cartesian case, for a 3×3 accelerated acquisition, suggesting an average SNR boost of about 40% for the wave-CAIPI technique. These measurements, however, were performed with a different undersampling pattern, coil setup, and different sequence parameters, tailored for head applications. Relevant sequence parameters that influence the g-factor in wave-CAIPI acquisitions are, for example, the resolution, the bandwidth, and the maximum wave amplitude, as systematically investigated in Polak et al[10] and Wang et al.[33] Further optimization potential of the present work lies in the wave-CAIPI parameters. The slew-rate limits of the used MR scanner would allow higher gradient wave amplitudes, which would further decrease the g-factor.[10,33] Regarding the g-factor map in Figure 9C, a further g-factor optimization with respect to the maximum gradient wave amplitude would be possible in regions with elevated g-factor, such as the center of the thorax, for instance. Moreover, the level of nerve stimulation is a limiting factor, as higher wave amplitudes generate more nerve stimulation. Slew rate or nerve-stimulation issues could be reduced by choosing a lower number of wave cycles.

Previous reports on wave encoding applied to motion-corrected, free-breathing abdominal imaging presented an enhanced performance in reducing aliasing and motion artifacts, compared with Cartesian sampling.[13] The proposed termination criterion for the iterative SENSE reconstruction estimated the noise level of a theoretically fully sampled acquisition in the image domain. The resulting noise estimate was used for all retrospectively accelerated data sets of the respective volunteer. A more elaborated termination criterion could, along sensitivity maps and noise correlations, also include the actual sampling pattern and thereby the sampling time of the individual undersampled data sets.

It was shown[15,17] that simple, linear phase encoding leads to large gaps in k-space after respiratory gating, entailing extensive undersampling artifacts in the image domain. Using the density-weighted phase-encoding scheme proposed in Breuer et al,[15] readout lines near the k-space center are measured more often, and large gaps in the k-space center are avoided. Use of the wave-CAIPI k-space trajectory further prevents large voids in k-space. Due to the helically shaped readout lines, undersampling results in a more homogeneous distribution of missing k-space samples, as all three dimensions in k-space are involved in undersampling. In contrast, undersampling in the Cartesian case takes place only in two dimensions, leaving the readout direction always fully sampled. As a result, the wave-CAIPI images exhibit a highly reduced artifact level, as shown in Figures 4 and 5. Residual undersampling artifacts are visible in the accelerated Cartesian images, which complicates vessel identification and delineation.

In Breuer et al,[15] full coverage of the lung was achieved in 3 minutes, using a randomized, self-gated and density-weighted Cartesian sequence. Calculations of the normalized mutual information displayed in Figure 6 and the image comparison in Figure 4 indicate that the image quality of a 3-minute Cartesian scan is comparable to the image quality of a 2-minute wave-CAIPI scan. Thus, the benefit of using the wave-CAIPI k-space trajectory can be traded for a reduced acquisition time or enhanced image quality, keeping the scan time constant. Using the wave-CAIPI technique, the SNR benefit could also be traded for higher temporal resolution of the respiratory cycle. Keeping the scan time constant, a higher number of (independent) breathing states implies an increased undersampling rate.

An interesting extension of the presented work would be to play out phase-encoding steps according to the actual current breathing state, as determined by the DC signal. Instead of prospectively defining a suitable order of the phase-encoding steps, the sampling patterns in each breathing state could thereby be adjusted as desired. Such an approach would, however, come at the expense of an unpredictable scan time.

5 | CONCLUSIONS

Quantitative image analysis, involving calculations of SNR, normalized mutual information and RMSE, demonstrated an enhanced image quality for the wave-CAIPI technique, compared with the Cartesian sequence in free-breathing, self-gated 4D lung MRI. The combination of density weighting and the wave-CAIPI k-space trajectory enables full coverage of the human lung in eight breathing states in only a few minutes.

ACKNOWLEDGMENTS

The authors thank Serge-Peer Ströhle for the valuable discussions.

CONFLICT OF INTEREST

J. A. J. Richter and M. Stich are now employees of Siemens Healthcare, Erlangen, Germany. Their contribution to the submitted work precedes their employment at Siemens. The university hospital würzburg received a research grant from Siemens Healthcare.

DATA AVAILABILITY STATEMENT

The source code for the iterative Conjugate Gradient SENSE reconstruction is publicly available at https://github.com/expRad/4d_lung. A volunteer 4D-lung MRI data set can be downloaded from zenodo.org (https://doi.org/10.5281/zenodo.3765168).

ORCID

Julian A. J. Richter https://orcid.org/0000-0001-7459-2086
Tobias Wech https://orcid.org/0000-0002-2813-7100
Andreas M. Weng https://orcid.org/0000-0001-8943-3539

REFERENCES

1. von Siebenthal M, Székely G, Gamper U, Boesiger P, Lomax A, Cattin P. 4D MR imaging of respiratory organ motion and its variability. *Phys Med Biol*. 2007;52:1547-1564.
2. Tokuda J, Morikawa S, Haque HA, et al. Adaptive 4D MR imaging using navigator-based respiratory signal for MRI-guided therapy. *Magn Reson Med*. 2008;59:1051-1061.
3. Arnold JFT, Mörchel P, Glaser E, Pracht ED, Jakob PM. Lung MRI using an MR-compatible active breathing control (MR-ABC). *Magn Reson Med*. 2007;58:1092-1098.
4. Fischer A, Weick S, Ritter CO, et al. SElf-gated Non-Contrast-Enhanced FUnctional Lung imaging (SENCEFUL) using a quasi-random fast low-angle shot (FLASH) sequence and proton MRI. *NMR Biomed*. 2014;27:907-917.
5. Weick S, Breuer FA, Ehses P, et al. DC-gated high resolution three-dimensional lung imaging during free-breathing. *J Magn Reson Imaging*. 2013;37:727-732.
6. Crowe ME, Larson AC, Zhang Q, et al. Automated rectilinear self-gated cardiac cine imaging. *Magn Reson Med*. 2004;52:782-788.
7. Mendes Pereira L, Wech T, Weng A, et al. UTE-SENCEFUL: First results for 3D high-resolution lung ventilation imaging. *Magn Reson Med*. 2019;81:2464-2473.
8. Bilgic B, Gagoski BA, Cauley SF, et al. Wave-CAIPI for highly accelerated 3D imaging. *Magn Reson Med*. 2015;73:2152-2162.
9. Cauley SF, Setsompop K, Bilgic B, Bhat H, Gagoski B, Wald LL. Autocalibrated wave-CAIPI reconstruction; Joint optimization of k-space trajectory and parallel imaging reconstruction. *Magn Reson Med*. 2017;78:1093-1099.
10. Polak D, Cauley S, Huang SY, et al. Highly-accelerated volumetric brain examination using optimized wave-CAIPI encoding. *J Magn Reson Imaging*. 2019;50:961-974.
11. Breuer FA, Moriguchi H, Seiberlich N, et al. Zigzag sampling for improved parallel imaging. *Magn Reson Med*. 2008;60:474-478.
12. Moriguchi H, Duerk JL. Bunched phase encoding (BPE): A new fast data acquisition method in MRI. *Magn Reson Med*. 2006;55:633-648.
13. Chen F, Zhang T, Cheng JY, Shi X, Pauly JM, Vasanawala SS. Autocalibrating motion-corrected wave-encoding for highly accelerated free-breathing abdominal MRI. *Magn Reson Med*. 2017;78:1757-1766.
14. Cheng JY, Zhang T, Ruangwattanapaisarn N, et al. Free-breathing pediatric MRI with nonrigid motion correction and acceleration. *J Magn Reson Imaging*. 2015;42:407-420.
15. Breuer K, Meyer CB, Breuer FA, et al. Stable and efficient retrospective 4D-MRI using non-uniformly distributed quasi-random numbers. *Phys Med Biol*. 2018;63:075002.
16. Kumar S, Rai R, Stemmer A, et al. Feasibility of free breathing lung MRI for radiotherapy using non-Cartesian k-space acquisition schemes. *Br J Radiol*. 2017;90:20170037.
17. Weick S, Völker M, Hemberger K, et al. Desynchronization of Cartesian k-space sampling and periodic motion for improved retrospectively self-gated 3D lung MRI using quasi-random numbers. *Magn Reson Med*. 2017;77:787-793.
18. Matsumoto M, Nishimura T. Mersenne twister: A 623-dimensionally equidistributed uniform pseudo-random number generator. *ACM Trans Model Comput Simul*. 1998;8:3-30.
19. Vannesjo SJ, Haeberlin M, Kasper L, et al. Gradient system characterization by impulse response measurements with a dynamic field camera. *Magn Reson Med*. 2013;69:583-593.
20. Vannesjo SJ, Graedel NN, Kasper L, et al. Image reconstruction using a gradient impulse response model for trajectory prediction. *Magn Reson Med*. 2016;76:45-58.
21. Campbell-Washburn AE, Xue H, Lederman RJ, Faranesh AZ, Hansen MS. Real-time distortion correction of spiral and echo planar images using the gradient system impulse response function. *Magn Reson Med*. 2016;75:2278-2285.
22. Stich M, Wech T, Slawig A, et al. Gradient waveform pre-emphasis based on the gradient system transfer function. *Magn Reson Med*. 2018;80:1521-1532.
23. Pruessmann KP, Weiger M, Börnert P, Boesiger P. Advances in sensitivity encoding with arbitrary k-space trajectories. *Magn Reson Med*. 2001;46:638-651.
24. Jackson JI, Meyer CH, Nishimura DG, Macovski A. Selection of a convolution function for Fourier inversion using gridding [computerised tomography application]. *IEEE Trans Med Imaging*. 1991;10:473-478.
25. Uecker M, Ong F, Tamir JI, et al. Berkeley advanced reconstruction toolbox. In: Proceedings of the 23rd Annual Meeting of ISMRM, article no, 2486. Toronto, Canada, 2015.
26. Robson PM, Grant AK, Madhuranthakam AJ, Lattanzi R, Sodickson DK, McKenzie CA. Comprehensive quantification of signal-to-noise ratio and g-factor for image-based and k-space-based parallel imaging reconstructions. *Magn Reson Med*. 2008;60:895-907.
27. Qu P, Zhong K, Zhang B, Wang J, Shen GX. Convergence behavior of iterative SENSE reconstruction with non-Cartesian trajectories. *Magn Reson Med*. 2005;54:1040-1045.
28. Pluim JPW, Maintz JBA, Viergever MA. Mutual-information-based registration of medical images: A survey. *IEEE Trans Med Imaging*. 2003;22:986-1004.
29. Strehl A, Ghosh J. Cluster ensembles—A knowledge reuse framework for combining multiple partitions. *J Mach Learn Res*. 2002;3:583-617.
30. Wolthaus JWH, Sonke J-J, van Herk M, et al. Comparison of different strategies to use four-dimensional computed tomography in treatment planning for lung cancer patients. *Int J Radiat Oncol Biol Phys*. 2008;70:1229-1238.
31. Wolthaus JWH, Schneider C, Sonke J-J, et al. Mid-ventilation CT scan construction from four-dimensional respiration-correlated CT scans for radiotherapy planning of lung cancer patients. *Int J Radiat Oncol Biol Phys*. 2006;65:1560-1571.
32. Heerkens HD, Hall WA, Li XA, et al. Recommendations for MRI-based contouring of gross tumor volume and organs at risk for radiation therapy of pancreatic cancer. *Pract Radiat Oncol*. 2017;7:126-136.
33. Wang H, Qiu Z, Su S, et al. Parameter optimization framework on wave gradients of Wave-CAIPI imaging. *Magn Reson Med*. 2020;83:1659-1672.

How to cite this article: Richter JAJ, Wech T, Weng AM, et al. Free-breathing self-gated 4D lung MRI using wave-CAIPI. *Magn Reson Med*. 2020;84:3223–3233. https://doi.org/10.1002/mrm.28383